Journal Syifa Sciences and Clinical Research (JSSCR)
Volume 7 Number 3, 2025
Journal Homepage: http://ejurnal.ung.ac.id/index.php/jsscr, E-ISSN: 2656-9612 P-ISSN:2656-8187
DOI: https://doi.org/10.37311/jsscr.v7i3.33990

Development of Nano-TiO_2 Activated Carbon as Antibacterial Agent in Hospital Waste

Binti Mu'arofah[1]*, Tri Ana Mulyati[2], Fery Eko Pujiono[3], Sri Wahyuni[4], Nurul Istiqomah[5]

[1] *Diploma (D3) Program in Medical Laboratory Technology, Institut Ilmu Kesehatan Bhakti Wiyata (IIK Bhakta), Kediri, Indonesia*
[2,3] *Bachelor of Pharmacy Program, Institut Ilmu Kesehatan Bhakti Wiyata (IIK Bhakta), Kediri, Indonesia.*
[4] *Applied Bachelor (D4) Program in Medical Laboratory Technology, Institut Ilmu Kesehatan Bhakti Wiyata (IIK Bhakta), Kediri, Indonesia.*
[5] *Diploma (D3) Program in Pharmacy, Institut Ilmu Kesehatan Bhakti Wiyata (IIK Bhakta), Kediri, Indonesia*

* *Corresponding Author. Email: binti.muarofah@iik.ac.id*

ABSTRACT

Hospital wastewater frequently harbors multidrug-resistant Gram-negative bacteria, motivating eco-benign materials that couple adsorption with antibacterial function. We prepared activated carbon from sugarcane bagasse by carbonization and KOH activation and modified it with nano-TiO_2 (target loadings 5 and 10 wt%). FTIR revealed interfacial Ti–O–C features (1695/1572 cm^{-1}) and Ti–O–Ti vibrations (682 cm^{-1}), XRD showed anatase reflections (2θ ≈ 25.2°, 37.7°, 48.1°, 53.8°, 55.0°), and SEM–EDX confirmed surface decoration with more homogeneous dispersion at lower TiO_2 and incipient agglomeration at higher loading. Antibacterial activity was assessed by agar well-diffusion on Mueller–Hinton Agar under dark incubation (37 °C, 24 h) against clinical isolates of *Escherichia coli*, *Klebsiella pneumoniae*, and *Pseudomonas aeruginosa*. Inhibition-zone ranges were 13.0–14.2 mm for *E. coli*, 10.0–14.5 mm for *K. pneumoniae* (carbon control highest), and 8.0–10.5 mm for *P. aeruginosa* (AC K(5)/Ti(10) largest). These species-dependent, moderate effects under non-photocatalytic conditions are consistent with interfacial acid–base/electrostatic interactions and adsorption rather than light-driven oxidation. Overall, TiO_2-modified, bagasse-derived activated carbon integrates adsorptive and antibacterial functions and is a promising candidate for hospital-wastewater treatment. Future work should optimize TiO_2 loading/immobilization, control pH/ionic strength, and evaluate performance under UV-A/visible illumination in continuous-flow systems to leverage adsorption–photocatalysis synergy.

Keywords:
nano-TiO_2; Activated carbon; Composite; Antibacterial activity; Hospital wastewater; Photocatalysis

Received:	*Accepted:*	*Online:*
2025-08-16	*2025-11-13*	*2025-11-28*

1. Introduction

Hospitals serve as facilities for healing and recovery. However, they can also become potential sources of infectious disease transmission. One of the major routes of disease spread is hospital wastewater, which has been shown to contain various pathogenic bacteria such as *Enterobacter cloacae*, *Bacillus* sp., *Klebsiella oxytoca*, and *Escherichia coli*. Previous studies have reported that the number of coliform bacteria in

hospital wastewater can reach up to 2.4 × 10^3 MPN/100 mL, indicating a high risk of environmental contamination and threats to public health [1],[2].

In Indonesia, hospital wastewater treatment generally relies on chemical disinfectants. Although effective, long-term use of these disinfectants can negatively impact the environment and promote the development of bacterial resistance to antibiotics. This condition necessitates the development of environmentally friendly antibacterial materials capable of addressing resistance issues [3].

One promising material is activated carbon, which possesses a large surface area and high porosity and can be synthesized from agricultural waste such as sugarcane bagasse. However, the antibacterial activity of activated carbon remains limited due to its weak mechanical properties. Conversely, nano-TiO_2 is well known for its photocatalytic activity that can damage bacterial cell walls, but it tends to aggregate, thereby reducing its effectiveness [4].

The modification of activated carbon with nano-TiO_2 is expected to overcome the limitations of each material. This combination has the potential to produce a composite material with both high adsorption capacity and enhanced antibacterial activity. Several studies have demonstrated the successful incorporation of TiO_2 into various matrices; however, research on the utilization of sugarcane bagasse–based activated carbon modified with nano-TiO_2 as an antibacterial agent for hospital wastewater treatment remains very limited. Therefore, this study was conducted to develop activated carbon derived from sugarcane bagasse modified with nano-TiO_2 and to evaluate its antibacterial activity against Gram-positive and Gram-negative bacteria isolated from hospital wastewater [4],[5],[6].

2. Methods

Study site and samples

Hospital wastewater used as the antibacterial test matrix was collected from Hospital "X" (Kediri City) following aseptic procedures and transported on ice for immediate processing. Clinical isolates of *Escherichia coli*, *Klebsiella pneumoniae*, and *Pseudomonas aeruginosa* were obtained from the same wastewater source and identified according to the local laboratory workflow as reported previously for this setting [3]. Sugarcane bagasse, used as the activated-carbon precursor, was sourced from Srikaton Village, Papar District, Kediri Regency, Indonesia, consistent with prior bagasse-to-carbon studies [5],[9],[10].

Preparation of biochar (carbonization)

Bagasse was thoroughly washed with tap water followed by distilled water, oven-dried (105 °C, 24 h), and milled. The feedstock was carbonized in a muffle furnace (400–900 °C, 1 h) under limited air access. The carbonized product was cooled in a desiccator and sieved to 100-mesh, following temperature windows commonly used for lignocellulosic carbons [5],[9],[10].

Chemical activation

Carbonized bagasse was chemically activated by immersion in 10% (w/v) KOH at a solid–liquid ratio of 1:5 (w/v) with magnetic stirring (24 h). The suspension was vacuum-filtered, repeatedly washed with hot distilled water to near-neutral pH, and oven-dried at 105 °C (24 h). KOH activation is a well-established route to increase microporosity and surface functionality in biomass-derived carbons [5], [9], [10].

TiO_2 modification of activated carbon

Activated carbon was modified using titanium(IV) tetraisopropoxide (TTIP) as a precursor to form TiO_2 on the carbon surface. Briefly, carbon was immersed in TTIP

solution to obtain targeted TiO_2 loadings of 5 wt% and 10 wt% at a solid–liquid ratio of 1:5 (w/v), stirred for 2 h, then thermally treated at 200 °C for 30 min to hydrolyze/condense the precursor. The solid was washed with distilled water and dried at 60 °C for 5 h, yielding composites designated $KATiO_2$-5 and $KATiO_2$-10. TiO_2 functionalization of carbon supports is a common strategy to couple adsorption with (photo)antibacterial functionality [4],[16],[21]

Safety note: TTIP is moisture-sensitive; all handling was performed in a fume hood with appropriate PPE.

Material characterization

Functional groups were analyzed by FTIR; crystalline phases by X-ray diffraction (XRD); and surface morphology/elemental composition by scanning electron microscopy coupled with energy-dispersive X-ray spectroscopy (SEM-EDX). These techniques provide complementary evidence of TiO_2 anchoring on carbon supports and are standard for AC/TiO_2 composites [4],[15],[21].

Antibacterial assay (well diffusion)

Antibacterial activity was assessed on Mueller–Hinton Agar (MHA). Inocula of *E. coli*, *K. pneumoniae*, and *P. aeruginosa* were prepared from fresh cultures, adjusted to 0.5 McFarland, and lawn-spread with sterile swabs; plates were allowed to dry for 10–15 min. Composite powders were UV-sterilized (30 min per side in a biosafety cabinet) and aseptically suspended in sterile physiological saline 0.90% (w/v) to 100 mg/mL. Wells (6 mm) were punched with a sterile borer; 50 µL of suspension was dispensed into each well with ≥ 24 mm spacing between wells to avoid overlapping diffusion. Controls were: negative—50 µL sterile saline; matrix—50 µL suspension of activated carbon without TiO_2 (100 mg/mL); positive—ciprofloxacin 5 µg disk (CLSI standard) placed on the same plate as a diffusion benchmark. Plates were incubated 24 h at 37 °C in the dark (no light activation). Inhibition zones were measured as edge-to-edge clear-halo diameter (mm) along three orthogonal axes using a digital caliper, and reported as mean ± SD from n = 3 independent plates per treatment. Use of carbon-based antibacterial references and TiO_2-containing materials aligns with prior antibacterial materials research [4],[15], [21].

Data processing and statistics

Numerical data are reported as mean ± SD from three independent plates per treatment. Inhibition zones were measured as edge-to-edge diameters (mm) and averaged per plate. Where applicable, between-group comparisons were evaluated using one-way ANOVA (or Kruskal–Wallis for non-normal data), followed by appropriate post-hoc tests at $\alpha = 0.05$. All figures and the schematic workflow are shown in **Figure 1** and subsequent figures.

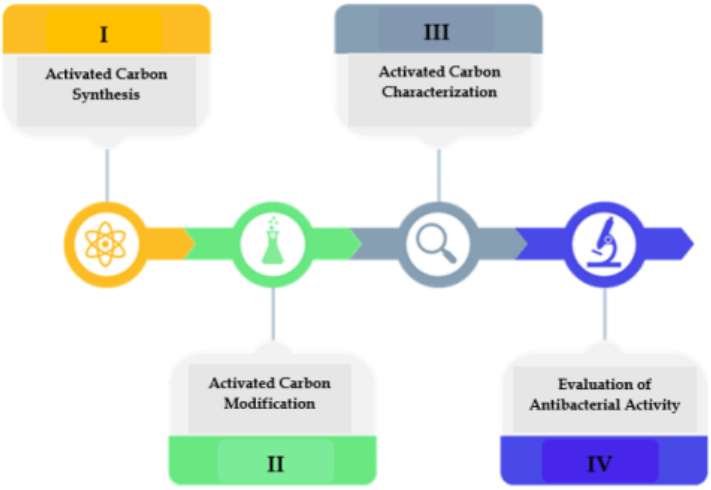

Figure 1. Workflow of TiO_2-modified activated carbon from sugarcane bagasse: (I) activated-carbon synthesis; (II) TiO_2 surface modification; (III) characterization (FTIR, XRD, SEM–EDX); (IV) antibacterial assay (agar well diffusion)

3. Result and Discussion

Carbonization, Activation, and TiO_2 Modification of Sugarcane Bagasse

This study converted sugarcane bagasse into activated carbon and subsequently deposited nano-TiO_2 to obtain antibacterial AC/TiO_2 composites. The workflow comprised raw-material preparation, carbonization, KOH activation, TiO_2 modification, physicochemical characterization (FTIR, XRD, SEM-EDX), and antibacterial evaluation against wastewater-derived clinical isolates. The stepwise mass balance (yield) across unit operations is summarized in **Table 1**; together with spectroscopic and microscopic evidence, these data substantiate successful conversion of bagasse into TiO_2-modified activated carbon suitable for downstream antibacterial testing [4],[6].

Table 1. Yield of Carbon, Activated Carbon, and TiO_2-Modified Carbon from Sugarcane Bagasse

Process Stage	Treatment/Condition	Mass Before (g)	Mass After (g)	Mass Loss (g)	Yield (%)	Remarks
Carbonization	400 °C, 1 h	70.40	23.95	46.45	34.02	Color changed from brown to black
Activation	5% KOH	8.84	6.21	2.63	70.24	Increased surface area
Activation	10% KOH	8.86	6.07	2.79	68.51	Slightly lower yield due to stronger etching
TiO_2 Modification	5% TiO_2	5.00	3.384	1.616	67.68	TiO_2 evenly dispersed on surface
TiO_2 Modification	10% TiO_2	5.00	3.673	1.327	73.46	Higher precursor may promote local clustering

Carbonization of bagasse at 400 °C for 1 h reduced the mass from 70.40 g to 23.95 g (yield 34.02%), accompanied by a color change from brown to black, indicating the removal of volatile fractions (hemicellulose, cellulose, lignin) and the enrichment of aromatic carbon domains that serve as proto-pores [6],[7],[8]. Subsequent chemical activation using KOH (5% and 10%, 1:5 w/v, 24 h) increased defect sites and accessible porosity typical of alkali-etched carbons; the mass yields were 70.24% (5% KOH) and 68.51% (10% KOH), with slightly greater mass loss at the higher KOH level due to intensified etching/gasification [4], [9], [10], [11].

Following activation, TiO_2 was introduced by immersing the carbon in a TTIP solution to target nominal loadings of 5 wt% and 10 wt%, followed by thermal treatment, washing, and drying. The composites are denoted $KATiO_2$-5 and $KATiO_2$-10. Mass retention during TiO_2 deposition suggested efficient anchoring at both loadings; however, higher precursor concentration may promote local clustering and partial pore blockage, a phenomenon commonly reported for oxide-decorated carbons and best examined via microscopy and diffraction rather than yield alone [12], [13]. As shown later (SEM-EDX/XRD), TiO_2 is present as anatase crystallites on the carbon surface, with dispersion quality varying by loading.

FTIR Characterization

Figure 2 compares the FTIR spectra of raw carbon (TK), KOH-activated carbon (KA), and TiO_2-modified activated carbons ($KATiO_2$-5 and $KATiO_2$-10). The raw carbon shows a broad band centered at 3390 cm^{-1} attributable to O–H stretching of physisorbed water and hydroxyl groups, together with weaker features typically observed for lignocellulosic carbons (C–H stretching near 2920/2850 cm^{-1}, carbonyl C=O around 1700–1725 cm^{-1}, aromatic C=C near 1600 cm^{-1}, and C–O/C–O–C in the 1000–1200 cm^{-1} window). After activation, the O–H envelope intensifies (**Figure 2b**), consistent with an increase in surface oxygenated functionalities and hydrogen-bonding capacity introduced by KOH etching/oxidation [4],[5].

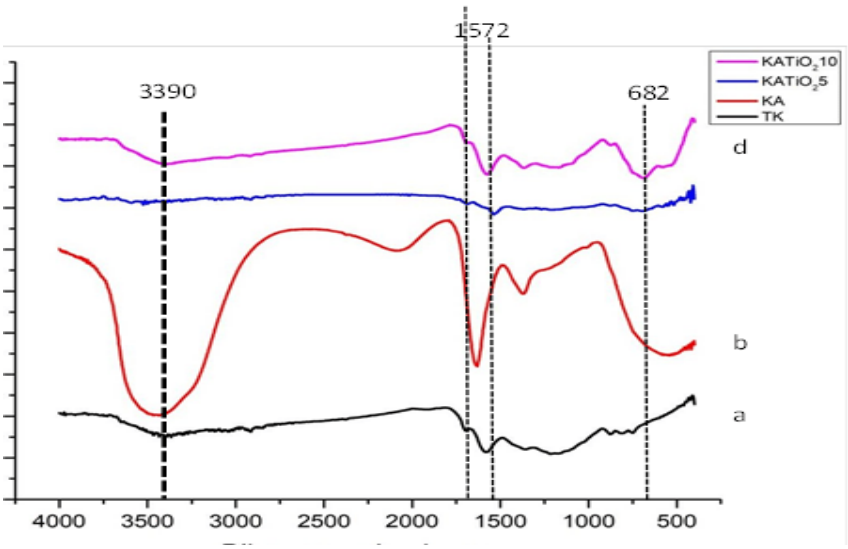

Figure 2. FTIR spectra of (a) TK (raw carbon), (b) KA (KOH-activated carbon), (c) $KATiO_2$-5, and (d) $KATiO_2$-10. Prominent bands: O–H (3390 cm^{-1}), Ti–O–C (1695/1572 cm^{-1}), and Ti–O–Ti (682 cm^{-1}).

Upon TiO_2 deposition, two interfacial signatures emerge: absorption at 1695 and 1572 cm^{-1} assigned to Ti–O–C linkages that indicate covalent/bridging interactions between titania and the activated-carbon surface [8],[14],[15]. In addition, a distinct band at 682 cm^{-1} corresponds to Ti–O–Ti vibrations of titania frameworks, confirming the incorporation of TiO_2 into the composite. Notably, $KATiO_2$-5 exhibits a relative decrease in the O–H band intensity compared to KA, suggesting partial masking/consumption of surface hydroxyls by TiO_2 anchoring. By contrast, $KATiO_2$-10 displays a stronger O–H envelope, plausibly reflecting the higher density of hydroxylated titania sites and enhanced water uptake at the composite surface at higher loading. Taken together, these spectral trends substantiate successful TiO_2 anchoring and interfacial bonding on KA while modulating the distribution of surface oxygen functionalities.

Because carbonyl and aromatic bands (1700 and 1600 cm^{-1}) can overlap with interfacial vibrations, the assignments above are interpreted in concert with the crystallographic and microstructural evidence presented later: anatase reflections in XRD and Ti mapping in SEM-EDX corroborate the presence and dispersion of titania domains on the carbon matrix [8],[14],[15]. From a structure–function standpoint, the formation of Ti–O–C bridges and the persistence of surface O-groups are relevant to the antibacterial response under dark conditions, as they govern acid–base interactions, hydration layers, and local microenvironments at the particle–cell interface (elaborated in subsection Antibacterial Activity of Nano-TiO_2-Modified Activated Carbon).

XRD Analysis

X-ray diffraction was recorded over 2θ = 5°–60° to compare the diffraction features of activated carbon (KA) and TiO_2-modified composites ($KATiO_2$-5 and $KATiO_2$-10). The KA pattern (**Figure 3a**) exhibits the broad, low-intensity halos at 2θ = 5°–10° and 20°–30° that are typical of disordered, turbostratic carbon, reflecting short-range ordering and low crystallinity in biomass-derived activated carbons [16]. This amorphous background provides a convenient "substrate" upon which oxide reflections can be identified.

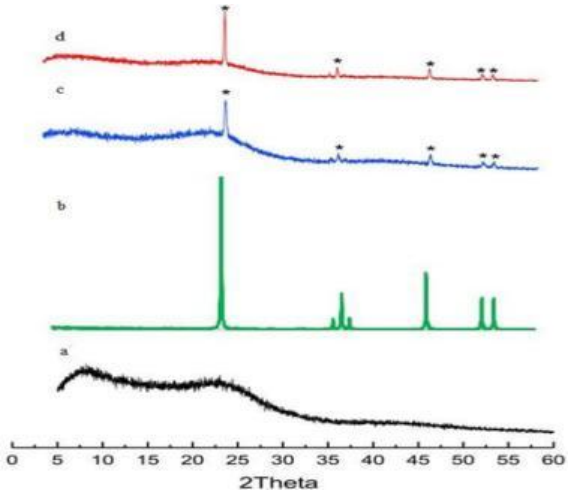

Figure 3. XRD patterns: (a) KA (activated carbon), (b) reference TiO_2 (JCPDS 21-1272), (c) $KATiO_2$-5, and (d) $KATiO_2$-10. Broad carbon halos (5°–10°, 20°–30°) and anatase reflections (25.2°, 37.7°, 48.1°, 53.8°, 55.0°) are indicated

After TiO_2 deposition, the diffractograms of $KATiO_2$-5 and $KATiO_2$-10 (**Figure 3c–d**) retain the amorphous carbon halos but additionally display sharp reflections at 2θ 25.2°, 37.7°, 48.1°, 53.8°, and 55.0°, matching the anatase phase of TiO_2 (JCPDS 21-1272) [4],[16]. No diagnostic peaks of rutile (e.g., 27.4°) or brookite are evident within the scanned window, indicating that anatase is the dominant crystalline phase under the present synthesis conditions. The relative intensities of anatase reflections increase from $KATiO_2$-5 to $KATiO_2$-10, consistent with a higher crystalline oxide fraction at the carbon surface. The peak positions remain unchanged with loading, suggesting that lattice parameters are not measurably perturbed (i.e., no obvious solid-solution effects), and that the differences arise primarily from phase fraction and domain growth rather than lattice distortion.

Taken together with FTIR (appearance of Ti–O–C and Ti–O–Ti vibrations) and SEM-EDX (surface Ti mapping), the XRD data confirm successful anchoring of crystalline anatase on the activated-carbon matrix [4],[16]. From a structure–function standpoint, an increased anatase signal with higher loading can provide more catalytically active domains, although—as discussed in SEM-EDX—excess loading may promote local agglomeration that reduces effective surface accessibility. This trade-off helps rationalize the antibacterial trends observed under dark conditions.

SEM–EDX Analysis

SEM micrographs reveal clear morphological transitions from the activated carbon matrix to the TiO_2-modified composites. The unmodified activated carbon (KA) shows a relatively layered, porous surface with open cavities typical of KOH-activated carbons, indicating a high external area and accessible porosity for subsequent surface reactions and adsorption (**Figure 4**).

After TiO_2 deposition, the surface texture becomes rougher with nanoscale particulates evident on the carbon framework. In $KATiO_2$-5, fine granular features are more uniformly distributed over the surface and within near-surface pores, consistent with a relatively homogeneous coverage at lower loading. By contrast, $KATiO_2$-10 exhibits denser clusters and partial agglomeration of TiO_2, with some pore mouths appearing less discernible, suggesting incipient pore blocking and particle coalescence at higher precursor concentration. Such loading-dependent aggregation behavior is frequently reported for oxide–decorated carbons and can diminish effective surface accessibility even as the oxide fraction increases [12],[13],[17],[18].

EDX spot/mapping analyses corroborate the SEM observations: Ti signals (e.g., Ti Kα) are detected on both composites, confirming successful immobilization of TiO_2 on the activated-carbon surface. Elemental maps qualitatively indicate a more even Ti distribution on $KATiO_2$-5, whereas $KATiO_2$-10 shows localized intensity "hot-spots," consistent with cluster formation. Together with FTIR assignments (Ti–O–C and Ti–O–Ti vibrations) and anatase reflections in XRD, these data verify that titania domains are anchored to the carbon matrix while highlighting the trade-off between oxide loading and dispersion quality [12],[13],[17],[18]. From a structure–function standpoint, improved dispersion at lower loading may support more uniform interfacial contact under dark antibacterial assays, whereas agglomeration at higher loading can reduce accessible interfacial area despite a greater crystalline TiO_2 fraction—an interpretation consistent with the inhibition-zone patterns discussed later.

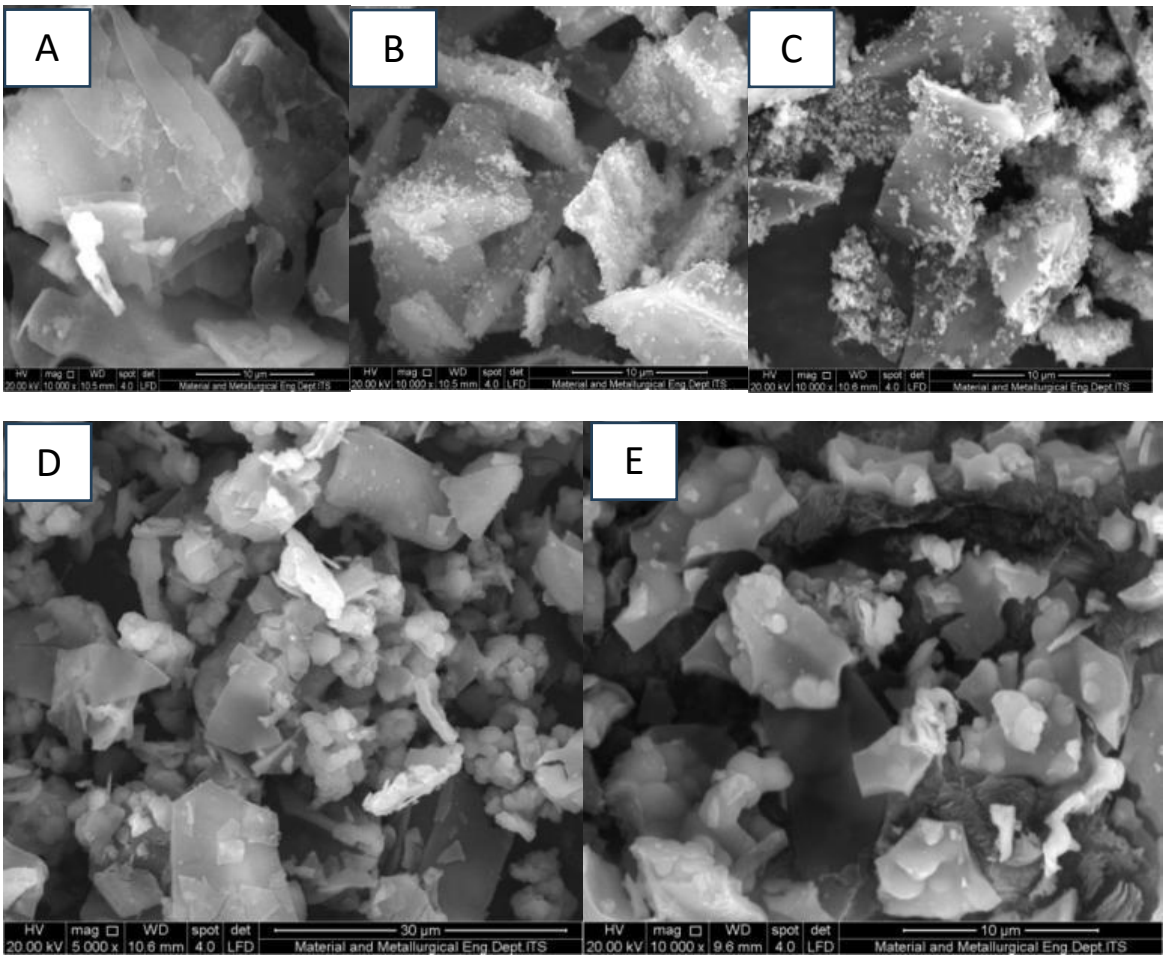

Note :

A. *KA (unmodified): layered porous morphology with open cavities.*
B. *KATiO$_2$-5 (overview): successful impregnation with finely dispersed particulates.*
C. *KATiO$_2$-10 (overview): denser deposition with evident particle clustering/agglomeration.*
D. *KATiO$_2$-10 (detail): localized clusters partially masking pore entrances.*
E. *KATiO$_2$-5 (detail): broadly distributed nanoscale features with limited agglomeration. EDX spectra/maps (not shown) confirm Ti presence on both composites, with more homogeneous Ti distribution in KATiO$_2$-5 and localized Ti "hot-spots" in KATiO$_2$-10 [12],[13],[17],[18].*

Figure 4. SEM micrographs and EDX confirmation of activated carbon before and after TiO_2 modification.

Antibacterial Activity of Nano-TiO_2-Modified Activated Carbon

Antibacterial efficacy was assessed by the agar well-diffusion assay on Mueller–Hinton Agar under dark incubation (37 °C, 24 h) against wastewater isolates of *Escherichia coli*, *Klebsiella* sp., and *Pseudomonas* sp. Inhibition halos were measured as edge-to-edge clear-zone diameters (mm) along three orthogonal axes and averaged per plate. Each treatment was tested on three independent plates; values are reported as mean ± SD (**Table 2**).

For *E. coli*, AC K(10)/Ti(10) yielded the largest zone (14.20 ± 0.30 mm; group a) and was statistically comparable to AC K(5)/Ti(5) (14.00 ± 0.25 mm; a^{b}). Both exceeded the carbon control (13.30 ± 0.30 mm; c^{d}) and AC K(5)/Ti(10) (13.00 ± 0.35 mm; d), while AC K(10)/Ti(3) (13.50 ± 0.20 mm; b^{e}) was intermediate. The pattern indicates that increasing TiO_2 can enhance activity against *E. coli*, although gains are not proportional across formulations.

Table 2. Inhibition zones (mm, mean ± SD; n = 3) of AC/TiO_2 composites

Sample (as tested)	*E. coli*	*Klebsiella* sp.	*Pseudomonas* sp.
Carbon (no TiO_2)	13.30 ± 0.30^{cd}	14.50 ± 0.40^{a}	9.50 ± 0.45^{b}
AC K(5)/Ti(5)	14.00 ± 0.25^{ab}	12.10 ± 0.30^{b}	8.00 ± 0.30^{c}
AC K(5)/Ti(10)	13.00 ± 0.35^{d}	12.00 ± 0.35^{b}	10.50 ± 0.50^{a}
AC K(10)/Ti(3)	13.50 ± 0.20^{bc}	12.50 ± 0.30^{b}	9.50 ± 0.40^{b}
AC K(10)/Ti(10)	14.20 ± 0.30^{a}	10.00 ± 0.25^{c}	8.00 ± 0.30^{c}

Note: Entries are mean ± SD from three independent plates; diameters are edge-to-edge (mm). Per species, between-group comparisons followed the plan in Data processing and statistics: one-way ANOVA with Tukey's test when assumptions were met, or Kruskal–Wallis with Dunn–Holm otherwise (a = 0.05). Superscripts indicate post-hoc groupings

For *Klebsiella* sp., the carbon control produced the largest diameter (14.50 ± 0.40 mm; a), significantly higher than all TiO_2-modified composites. AC K(5)/Ti(5) (12.10 ± 0.30 mm), AC K(5)/Ti(10) (12.00 ± 0.35 mm), and AC K(10)/Ti(3) (12.50 ± 0.30 mm) clustered together (group b), whereas AC K(10)/Ti(10) was the lowest (10.00 ± 0.25 mm; c). Under dark conditions, this underscores the dominant contribution of the activated-carbon scaffold via adsorption for *Klebsiella*.

For *Pseudomonas* sp., responses were the smallest overall and slightly more variable. AC K(5)/Ti(10) achieved the largest zone (10.50 ± 0.50 mm; a); the carbon control (9.50 ± 0.45 mm; b) and AC K(10)/Ti(3) (9.50 ± 0.40 mm; b) formed a middle tier, while AC K(5)/Ti(5) (8.00 ± 0.30 mm; c) and AC K(10)/Ti(10) (8.00 ± 0.30 mm; c) were equivalently smallest. This species-dependent resistance is congruent with the robust outer membrane and biofilm propensity of *Pseudomonas* under non-photocatalytic testing.

Because assays were conducted without light activation, the observed effects are best attributed to interfacial phenomena—specifically acid–base/electrostatic interactions and local adsorption–dehydration at the particle–cell boundary—and to how bulk pH positions the system relative to the TiO_2 point of zero charge, which modulates surface charge and cell–surface attraction [19], [20]. In parallel, SEM–EDX shows loading-dependent agglomeration at higher Ti contents, reducing accessible interfacial area; together, these features explain the absence of a monotonic relationship between TiO_2 fraction and antibacterial performance and the competitive outcomes achieved by better-dispersed, lower-loading composites [11], [21].

Translating these findings to practice, hospital-wastewater treatment should prioritize a continuous-flow train that marries front-end adsorption on activated carbon with downstream TiO_2 activation under UV-A/visible light, so that adsorptive preconcentration at the solid–liquid interface is followed by an oxidative step that damages envelopes and limits regrowth. Performance can be stabilized by routine control of pH and ionic strength to favor attractive surface interactions [19], [20] and by limiting particle agglomeration through optimized Ti loading or immobilization within a porous matrix, approaches consistent with adsorption-assisted photocatalysis reported for complex effluents [11], [15], [22].

This study has several limitations that restrict the interpretation of its findings. Antibacterial assays were performed under dark conditions, so the observed effects primarily reflect interfacial mechanisms—adsorption, acid–base/electrostatic interactions, and local dehydration—rather than TiO_2-driven photocatalysis. The well-diffusion format is intrinsically sensitive to particle/agglomerate diffusion and agar properties and does not provide pharmacodynamic metrics such as MIC, MBC, or time–kill kinetics. Replication was limited (n = 3 plates per treatment) without an a priori

power analysis, which reduces sensitivity to small between-group differences and widens uncertainty around effect estimates. Materials characterization was not exhaustive: surface area/porosity (BET), surface charge (zeta potential/point of zero charge), high-resolution surface chemistry (XPS), optical properties (DRS UV–Vis), hydrodynamic size distribution (DLS), and Ti leaching tests were not included, constraining structure–function inference and stability assessment. On the biological side, testing covered *E. coli*, *Klebsiella* sp., and *Pseudomonas* sp. from a single wastewater source without mature-biofilm assays, molecular typing, or systematic control of pH, ionic strength, and dissolved organics to emulate real effluent variability, which limits generalizability. Finally, process-level considerations—adsorbent regeneration, mechanical robustness under hydraulic shear, long-term performance in flow, and potential cyto-/ecotoxicity of residues—were not evaluated, leaving important questions about external validity and field-scale feasibility.

4. Conclusion

Activated carbon from sugarcane bagasse was successfully prepared by carbonization and KOH activation, then modified with nano-TiO_2. FTIR and XRD verified Ti–O–C interfacial bonding and anatase TiO_2, while SEM–EDX showed titania decorating the carbon surface with more homogeneous dispersion at lower loading and incipient agglomeration at higher loading. Under dark, agar well-diffusion conditions, antibacterial effects were moderate and species-dependent: AC K(10)/Ti(10) yielded the largest zone for *E. coli*; the carbon control was highest for *Klebsiella* sp.; and responses were smallest for *Pseudomonas* sp., with AC K(5)/Ti(10) performing best. These outcomes indicate that—in the absence of light—performance is governed mainly by interfacial adsorption and acid–base/electrostatic interactions rather than photocatalysis. Future research include optimizing TiO_2 loading and immobilization to minimize agglomeration while preserving accessible interface; evaluating performance under UV-A/visible illumination and in continuous-flow systems that couple front-end adsorption with downstream photocatalysis; tuning pH and ionic strength to favor cell–surface attraction; expanding the microbial panel to additional pathogens and mature biofilms; and reporting quantitative pharmacodynamic endpoints (MIC, MBC, time–kill) alongside ROS measurements to elucidate adsorption–photocatalysis synergy and operational stability/reusability.

Acknowledgements:

The authors extend their sincere appreciation to the hospital administrators in Kediri City for logistical support, to the microbiology laboratory personnel at Bhakti Wiyata Health Sciences Institute, for expert technical assistance for their contributions to sample collection and analysis.

Conflicts of Interest:

The author declares that there are no conflicts of interest in this research.

References

[1] J. C. A. Ranti, H. B. Sutanto, and G. Prihatmo, "Effectiveness of a constructed wetland system in reducing pathogenic bacteria in hospital wastewater," 2020. [Online]. Available:

[2] J. R. Lingkungan and C. Winarti, "Reduction of total coliform bacteria in hospital wastewater by UV irradiation time," n.d. [Online]. Available:

[3] T. A. Mulyati, B. Mu'arofah, F. E. Pujiono, and R. Alrayan, "Identification of pathogenic bacteria in liquid waste from 'X' Hospital in Kediri City," *Ad-Dawaa' Journal of Pharmaceutical Sciences*, pp. 109–116, Nov. 2024. [Online]. Available: https://doi.org/10.24252/djps.v7i2.50196

[4] B. F. Bukit, E. Frida, S. Humaidi, and P. Sinuhaji, "Self-cleaning and antibacterial activities of textiles using nanocomposite oil palm boiler ash (OPBA), TiO_2 and chitosan as coating," *South African Journal of Chemical Engineering*, vol. 41, pp. 105–110, Jul. 2022. [Online]. Available: https://doi.org/10.1016/j.sajce.2022.05.007

[5] N. Asbih, I. Yanti, and W. Wicaksono, "Synthesis and application of TiO_2/activated carbon from sugarcane bagasse for photocatalytic degradation of batik wastewater," *AIP Conference Proceedings*, vol. 3027, no. 1, Art. 050019, 2024. [Online]. Available: https://doi.org/10.1063/5.0204759

[6] G. Ge *et al.*, "Green synthesis of nitrogen-doped carbon dots from fresh tea leaves for selective Fe^{3+} detection and cellular imaging," *Nanomaterials*, vol. 12, no. 6, Mar. 2022. [Online]. Available: https://doi.org/10.3390/nano12060986

[7] A. J. Romero-Anaya, M. D. González, J. Granados-Reyes, L. E. Arrieche-Hernández, and Y. Cesteros, "Faster microwave-assisted synthesis of microspherical carbons from commercial and biomass-derived carbohydrates," *Catalysts*, vol. 15, no. 9, Sep. 2025. [Online]. Available: https://doi.org/10.3390/catal15090885

[8] L. K. Sakti, D. R. Eddy, M. D. Permana, M. L. Firdaus, Y. Deawati, and I. Rahayu, "Utilizing TiO_2 photocatalysis and natural SiO_2 superhydrophilicity synergy to improve self-cleaning activity in cotton fabric," *Cellulose*, vol. 31, pp. 5885–5898, 2024. [Online]. Available: https://doi.org/10.1007/s10570-024-05938-1

[9] K. Javidi Alsadi and N. Esfandiari, "Synthesis of activated carbon from sugarcane bagasse and application for mercury adsorption," *Pollution*, vol. 5, no. 3, pp. 585–596, 2019. [Online]. Available: https://doi.org/10.22059/poll.2019.269364.540

[10] K. Y. Foo, L. K. Lee, and B. H. Hameed, "Preparation of activated carbon from sugarcane bagasse by microwave-assisted activation for the remediation of semi-aerobic landfill leachate," *Bioresource Technology*, vol. 134, pp. 166–172, 2013. [Online]. Available: https://doi.org/10.1016/j.biortech.2013.01.139

[11] A. R. Gintu and D. Puspita, "Synthesis and characterization of carbon nanotubes (CNTs) from teak wood charcoal and their application as antibacterial active material," *Jurnal Kimia Riset*, vol. 5, no. 2, pp. 127–133, Dec. 2020. [Online]. Available: https://doi.org/10.20473/jkr.v5i2.22505

[12] A. K. H. A. A. Roquia and B. H. A. Alhasmi, "Synthesis and characterisation of carbon nanotubes from *Juglans regia* (walnut) shells waste," *Bashaier Hamed Abdullah Alhasmi*, vol. 29, no. 11, pp. 1–8, Mar. 2021. [Online]. Available: https://doi.org/10.1080/1536383X.2021.1900123

[13] Z. Zhou, X. Zhang, B. Ma, M. Chen, and D. Chen, "Fabrication of superhydrophobic PDMS/TiO_2 composite coatings with corrosion resistance," *Surface Innovations*, vol. 11, nos. 1–3, pp. 195–208, May 2022. [Online]. Available: https://doi.org/10.1680/jsuin.21.00067

[14] X. Chen, Y. Pei, X. Wang, W. Zhou, and L. Jiang, "Response surface methodology—central composite design optimization sugarcane bagasse activated carbon under varying microwave-assisted pyrolysis conditions," *Processes*, vol. 12, no. 3, Art. 497, 2024. [Online]. Available: https://doi.org/10.3390/pr12030497

[15] M. E. M. Nor, N. Hussin, M. A. H. Salahuddin, A. H. A. Samah, M. F. Towhid, and M. F. M. Radzi, "Evaluation of phenolic content and antibacterial activity of coconut (*Cocos nucifera* L.) shell and coir powder in different extraction solvents," *Journal of Tropical Plant Physiology*, vol. 15, no. 1, p. 9, Jun. 2023. [Online]. Available: https://doi.org/10.56999/jtpp.2023.15.1.28

[16] F. E. Pujiono, T. A. Mulyati, and M. N. Fizakia, "Activated carbon of coconut shell modified TiO_2 as a batik waste treatment," *Jurnal Riset Teknologi Pencegahan Pencemaran Industri*, vol. 11, no. 2, pp. 1–10, Nov. 2020. [Online]. Available: https://doi.org/10.21771/jrtppi.2020.v11.no2.p1-10

[17] A. Rahmawati, F. Robbika, and Yuafni, "Preparation of activated carbon from sugarcane bagasse using microwave-assisted $ZnCl_2$ chemical activation: Optimization and characterization study," *Pertanika Journal of Science & Technology*, vol. 32, no. 1, pp. 419–436, 2024. [Online]. Available: https://doi.org/10.47836/pjst.32.1.22

[18] K. F. Salama, R. AlJindan, A. Alfadhel, S. Akhtar, and E. A. Al-Suhaimi, "Enhanced antimicrobial performance of textiles coated with TiO_2 nanoparticles," *Journal of Industrial Textiles*, early access, 2024. [Online]. Available: https://doi.org/10.1177/15280837241233743

[19] A. R. Gintu and D. Puspita, "Synthesis and characterization of carbon nanotubes (CNTs) from teak wood charcoal and their application as antibacterial active material," *Jurnal Kimia Riset*, vol. 5, no. 2, pp. 127–133, Dec. 2020. [Online]. Available: https://doi.org/10.20473/jkr.v5i2.22505

[20] F. Shen, Z. Lu, K. Yan, K. Luo, S. Pei, and P. Xiang, "Synthesis and properties of carbon quantum dots as an antimicrobial agent and detection of ciprofloxacin," *Scientific Reports*, vol. 15, no. 1, Dec. 2025. [Online]. Available: https://doi.org/10.1038/s41598-025-14383-4

[21] E. Burchacka, K. Pstrowska, M. Bryk, F. Maciejowski, M. Kułażyński, and K. Chojnacka, "Properties of activated carbons functionalized with an antibacterial agent and a new SufA protease inhibitor," *Materials*, vol. 16, no. 3, Feb. 2023. [Online]. Available: https://doi.org/10.3390/ma16031263

[22] R. Masevani, R. Kurniati, J. S. Fitri, A. A. Dicken, and D. Islami, "The use of palm oil shell waste combined with *Aloe vera* ethanol extract as antibacterial agent," *Journal of Pharmacy and Science*, vol. 7, no. 1, pp. 95–104, Dec. 2023. [Online]. Available: https://doi.org/10.36341/jops.v7i1.4100